0026-895X/08/7304-1244–1253$20.00
MOLECULAR PHARMACOLOGY
Copyright © 2008 The American Society for Pharmacology and Experimental Therapeutics
Mol Pharmacol 73:1244–1253, 2008

Vol. 73, No. 4
41319/3315813
Printed in U.S.A.

BYK191023 (2-[2-(4-Methoxy-pyridin-2-yl)-ethyl]-3*H*-imidazo[4,5-*b*]pyridine) Is an NADPH- and Time-Dependent Irreversible Inhibitor of Inducible Nitric-Oxide Synthase

Mauro Tiso,[1] Andreas Strub, Christian Hesslinger, Claire T. Kenney, Rainer Boer, and Dennis J. Stuehr

Department of Pathobiology, Lerner Research Institute, Cleveland Clinic, Cleveland, Ohio (M.T., C.T.K., D.J.S.); and the Department of Biochemistry, Nycomed, Konstanz, Germany (A.S., C.H., R.B.)

Received August 29, 2007; accepted January 4, 2008

ABSTRACT

Imidazopyridine derivates were recently shown to be a novel class of selective and arginine-competitive inhibitors of inducible nitric-oxide synthase (iNOS), and 2-[2-(4-methoxy-pyridin-2-yl)-ethyl]-3*H*-imidazo[4,5-*b*]pyridine (BYK191023) was found to have very high selectivity in enzymatic and cellular models (*Mol Pharmacol* **69:**328–337, 2006). Here, we show that BYK191023 irreversibly inactivates murine iNOS in an NADPH- and time-dependent manner, whereas it acts only as a reversible L-arginine-competitive inhibitor in the absence of NADPH or during anaerobic preincubation. Time-dependent irreversible inhibition by BYK191023 could also be demonstrated in intact cells using the RAW macrophage or iNOS-overexpressing human embryonic kidney 293 cell lines. The mechanism of BYK191023 inhibition in the presence of NADPH was studied using spectral, kinetic, chromatographic, and radioligand binding methods. BYK191023-bound iNOS was spectrally indistinguishable from L-arginine-bound iNOS, pointing to an interaction of BYK191023 with the catalytic center of the enzyme. [^{3}H]BYK191023 was recovered quantitatively from irreversibly inactivated iNOS, and no inhibitor metabolite was detected by high-performance liquid chromatography (HPLC). Size exclusion chromatography revealed only about 20% iNOS dissociation into monomers. Furthermore, HPLC and spectrophotometric analysis showed that the irreversible inhibition was associated with loss of heme from iNOS and a reduced ability to form the distinctive ferrous heme-CO complex (cytochrome P450). Thus, enzyme inactivation is mainly caused by heme loss, and it occurs in the inhibitor-bound enzyme in the presence of electron flux from NADPH.

NO is a highly diffusible biological messenger generated by nitric-oxide synthases (EC1.14.13.39; NOS), a family of enzymes that catalyze the NADPH-dependent conversion of L-arginine to L-citrulline and NO in a two-step process (Stuehr, 1999). In mammalian cells, three NOS isozymes [inducible (iNOS), neuronal (nNOS), and endothelial (eNOS)] evolved to have significant functional differences despite having considerable sequence homology (Michel and Feron, 1997). Each NOS isoform is a homodimeric hemoprotein made up of two separate domains connected by a calmodulin (CaM) binding polypeptide. The oxygenase domain contains sites for iron protoporphyrin IX (heme), 6R-tetrahydrobiopterin (H_4B), and L-arginine (Arg), whereas the reductase domain contains binding sites for FAD, FMN, and NADPH. During NO biosynthesis, the electron flux in the NOS enzymes goes via NADPH → FAD → FMN through the reductase domain of one monomer to the heme iron in the oxygenase domain of the second monomer (Alderton et al., 2001). Therefore, NOS is active only when the two monomers associate into a homodimeric protein. Under normal conditions, NO is released in small amounts (picomolar to nanomolar) by nNOS and eNOS, and it has a central role in the regulation of vasodilation and in neurotransmission. Pathological effects can occur either when NO production is lower or higher than normal, and NO has been involved in a wide range

This work was supported by ALTANA Pharma AG.
[1] Current affiliation: Vascular Medicine Branch, National Heart Lung and Blood Institute, National Institutes of Health, Bethesda, Maryland
Article, publication date, and citation information can be found at http://molpharm.aspetjournals.org.
doi:10.1124/mol.107.041319.

ABBREVIATIONS: NOS, nitric-oxide synthase(s); iNOS, inducible nitric-oxide synthase; nNOS, neuronal nitric-oxide synthase; eNOS, endothelial nitric-oxide synthase; CaM, calmodulin; H_4B, (6*R*)-5,6,7,8-tetrahydro-L-biopterin; Arg, L-arginine; BYK191023, 2-[2-(4-methoxy-pyridin-2-yl)-ethyl]-3*H*-imidazo[4,5-b]pyridine; 1400W, *N*-(3-(aminomethyl)benzyl)acetamidine; EPPS, 4-(2-hydroxyethyl)-1-piperazinepropanesulfonic acid; BSA, bovine serum albumin; SOD, superoxide dismutase; HEK, human embryonic kidney; DMEM, Dulbecco's modified Eagle's medium; FCS, fetal calf serum; IFN, interferon; LPS, lipopolysaccharide; HPLC, high-performance liquid chromatography; PVDF, polyvinylidene difluoride; P450, cytochrome P450; P420, cytochrome P420; ROS, reactive oxygen species.

of disorders (e.g., sepsis, hypoxia-ischemia, stroke, asthma, and chronic neurodegenerative diseases) (Moore et al., 2005). Overproduction of NO by inducible NOS during inflammation and immune activation leads to hypotension, vasodilatation, and disruption of cell metabolism, and it is also suggested to be involved in a variety of disease processes (Li and Forstermann, 2000; Xu et al., 2002). iNOS activity has also been detected in many human tumors, although its function is poorly understood (Lechner et al., 2005). The tight control of NOS isoform activity and NO concentration in different tissues has made it very difficult to develop NOS inhibitors clinically successful as drugs, although various inhibitors have been essential to evaluate the role of NO in pathophysiological processes (Hobbs et al., 1999). For example, a range of structurally related arginine analogs have been found to inhibit NOS enzymes, although possessing minimal isoenzyme selectivity (Alderton et al., 2001). However nNOS- or iNOS-selective inhibitors have been proposed to be useful, respectively, in treating stroke and neurodegenerative diseases and to control inflammatory responses, septic shock, and cancer. For this reason, the development of isoform-selective NOS inhibitors as therapeutic agents has become an area of active research and in recent years different approaches have been successful to obtain highly selective inhibitors that were made available for clinical studies (Garvey et al., 1997; Paige and Jaffrey, 2007). Recently, imidazopyridine derivates have been identified as a novel class of highly selective iNOS inhibitors (Strub et al., 2006). BYK191023, a selected member of this class (chemical structure displayed in Fig. 1), has been characterized as an Arg-competitive inhibitor in vitro and in vivo (Lehner et al., 2006; Strub et al., 2006); however, the molecular mechanism by which BYK191023 inhibits iNOS remains unclear. In this study, we observed two types of inhibition depending on the presence or absence of NADPH. In its absence, BYK191023 acts as a reversible Arg-competitive inhibitor, but it induces a time- and oxygen-dependent irreversible inactivation of iNOS in the presence of electron transfer from NADPH to the heme in the iNOS oxygenase domain.

Materials and Methods

Materials. All reagents were obtained from Sigma-Aldrich (St. Louis, MO) or from sources reported previously (Tiso et al., 2005). Hemin and biliverdin IXa were purchased from ICN Pharmaceuticals (Solon, OH), 1400W was obtained from Cayman Chemical (Ann Arbor, MI), and BYK191023 was provided by ALTANA Pharma AG (Konstanz, Germany). Superdex HG200 gel filtration columns were purchased from Amersham Biosciences (Chalfont St. Giles, Buckinghamshire, UK). UV-visible spectra and steady-state kinetic data were recorded on a UV-2401PC (Shimadzu, Kyoto, Japan) or Cary 100 Bio (Varian, Inc., Palo Alto, CA) spectrophotometer.

General Methods. The buffer used for all experiments and protein purifications (buffer A), unless noted otherwise, contained 40 mM EPPS, pH 7.6, 10% glycerol, and 150 mM NaCl. When necessary, samples were made anaerobic in an airtight cuvette by repeated cycling of vacuum followed by a positive pressure of deoxygenated nitrogen. Stock solutions of 10 mM BYK191023 were made in dimethyl sulfoxide, and they were stored at −20°C. Total protein concentrations were determined by the Bradford protein assay using bovine serum albumin (BSA) as standard. All plots and data fitting were done using Origin 7.5 (OriginLab Corp., Northampton, MA).

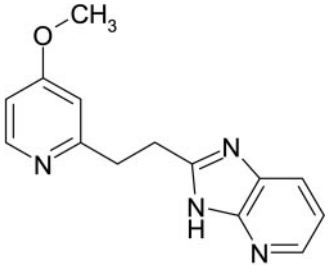

Fig. 1. Chemical structure of BYK191023.

NOS Isozymes Expression and Purification. Wild-type murine iNOS and nNOS full-length or oxy proteins were overexpressed in *Escherichia coli* strain BL21(DE3) containing a His_6 tag in the N termini to aid purification in a nickel-resin affinity column. Sequential chromatography on a 2′,5′-ADP Sepharose affinity column lead to purified protein (assessed by SDS-polyacrylamide gel electrophoresis) as described previously (Stuehr, 1996). In some cases, iNOS was purified by including H_4B but omitting Arg in all buffers used, and this form was denoted iNOS (+,−). All proteins were dialyzed against buffer A (see *Materials*) containing 10 μM H_4B, and they were stored in aliquots at −80°C. Enzyme concentration was determined by quantification of heme protein content as evidenced through the formation of the ferrous heme-CO adduct with an absorption maxima at 444 nm (Adak et al., 1999).

NOS Activity Assay. The rate of NO synthesis was determined by monitoring the NO-mediated conversion of oxyhemoglobin to methemoglobin at 401 nm as described previously (Tiso et al., 2005) using as extinction coefficient ε_{401} = 38 mM^{-1} cm^{-1}. The oxyhemoglobin assay contains 50 nM enzyme, 100 μM NADPH, 0.3 mM dithiothreitol, 4 μM FAD, 4 μM FMN, 10 μM H_4B, 100 units/ml superoxide dismutase (SOD) and catalase, 5 to 10 μM oxyhemoglobin, and 100 μM Arg (or otherwise indicated) in a total volume of 700 μl of 40 mM EPPS, pH 7.6. The initial rate of NADPH oxidation was similarly measured by the absorbance decrease at 340 nm under identical conditions in the presence of oxyhemoglobin and by using an extinction coefficient of ε_{340} = 6.2 mM^{-1} cm^{-1}. For nNOS, the assay solution contained also 150 mM NaCl to optimize the activity assay.

NADPH- and Time-Dependent Inhibition of NOS with BYK191023. The time-dependent onset of inhibition was examined by preincubating the enzymes in the presence or absence of inhibitor NADPH and cofactors and then by transferring aliquots of the reaction to the NOS activity assay mixture. In general, an air-saturated solution of 2.5 μM iNOS (+,−) in 40 mM EPPS, pH 7.6, containing 10 μM BYK191023, 0.15 mg/ml BSA, 10 μM H_4B, and 100 unit/ml SOD, and 25 unit/ml catalase when indicated, was incubated with 1 mM NADPH (administrated in 2 aliquots of 500 μM at time 0 and 15 min) in a total volume of 150 μl at room temperature. The solution was kept in equilibrium with air by mechanical methods. Aliquots (20 μl) of the preincubation mixture were transferred to the oxyhemoglobin assay mixture to monitor the NADPH consumption and NO synthesis at determined time points. The same conditions were used for nNOS but including 20 μM calmodulin and 0.8 mM $CaCl_2$ in the preincubation mixture. The enzyme was preincubated without BYK191023 as a negative control for inhibition, and we use the time-dependent iNOS-selective inhibitor 1400W as a positive control.

Enzyme Inhibition under Anaerobic Condition. Concentrated BYK191023, NADPH, and iNOS (+,−) (prepared as described above) were separately made anaerobic. Known amounts were transferred in a septum-sealed quartz cuvette containing anaerobic buffer to duplicate concentrations used in aerobic experiments. Aliquots from this cuvette were removed using an airtight syringe and tested for NO synthesis with the oxyhemoglobin assay at fixed time points. Time-dependent inhibition was evaluated in the presence or in the absence of 1 mM NADPH. Negative and positive controls of inhibition were replicated in anaerobic conditions. NADPH consumption during anaerobic preincubation was estimated by its absorbance decrease at 340 nm.

Interaction between BYK191023 and iNOS. UV-visible spectra were recorded after mixing known amounts of inhibitors with 4 μM iNOS (+,−) oxy or full-length. Spectral changes resulting from the association of BYK191023 with the enzyme were observed, and the difference spectrum between the two conditions was calculated.

Determination of Apparent k_{off}. Enzyme and inhibitor were mixed, and they were allowed to bind until equilibrium. To induce displacement of the inhibitor, excess imidazole (25 mM) was added, and the absorbance decrease of the high-spin peak (396 nm) was spectroscopically monitored versus time. The data obtained were fitted using a first-order exponential decay equation.

Time- and Concentration-Dependent Irreversible Inhibition of iNOS in HEK293 iNOS Cells. iNOS-overproducing HEK293 cells were obtained from Dr. S. Strand (Johannes Gutenberg University, Mainz, Germany), and they were cultivated in Arg-free DMEM supplemented with 50 μM Arg and 0.5% FCS as described previously (Strub et al., 2006). To induce the expression of human iNOS, cells were seeded at 10^6 cells/well in six-well microtiter plates and stimulated with 3 μM ponasterone A (Sigma-Aldrich) for 20 to 24 h. To analyze the time-dependent irreversible inhibition of iNOS enzyme activity, cells were incubated with varying concentrations of BYK191023 for the indicated time points, scrapped, and washed three times with DMEM to remove essentially all unbound inhibitor. Next, cells were lysed with 1% Triton X-100. iNOS enzyme activity was determined in the lysates essentially as described previously (Strub et al., 2006), using the L-[^{3}H]arginine method. The efficacy of removing unbound inhibitor was determined using 25 nM [^{3}H]BYK191023 in a separate experiment, with identical wash steps. The efficacy was calculated from the residual radioactivity after one to four subsequent wash steps.

Time-Dependent Irreversible Inhibition of Cellular iNOS in RAW Cells. RAW264.7 cells (mouse macrophage cell line; American Type Culture Collection, Manassas, VA) were cultured in DMEM, 10% FCS, 1% L-glutamine, and 1% penicillin/streptomycin. After reaching confluence, cells were stimulated by the addition of 100 U/ml IFN-γ and 1 μg/ml LPS for 18 h. Cells were scrapped, and 10^6 cells/ml were resuspended in serum- and Arg-reduced DMEM, 0.5% FCS, 1% L-glutamine, 1% penicillin/streptomycin, and 100 μM Arg. Cells were incubated with 100 μM BYK191023 for times indicated, and thereafter they were resuspended in assay buffer (phosphate-buffered saline, pH 7.4, 1 mM $CaCl_2$, 1 mM $MgCl_2$, and 100 μM Arg) to determine rates of NO release. Final concentration of dimethyl sulfoxide was 1% in all samples.

Direct Measurement of Cellular NO Release. NO release was measured using a NO-selective microelectrode (ami NO-700; Innovative Instruments Inc., Tampa, FL), and an amplifier (inNO-II meter; Innovative Instruments Inc.). The electrode was calibrated by producing standardized concentrations of NO in 0.5% (w/v) potassium iodide in 0.1 M H_2SO_4 from $NaNO_2$ standards. Determination of nitric oxide was performed at 37°C using 500 μl of stirred cell suspension in assay buffer (10^6 cells/ml) using a platelet aggregometer (PAP-4; MöLab, Hilden, Germany). NO release was quantified from the signal (maximum) that could be reduced by specific iNOS inhibition compared with the signal obtained from buffer as background control.

Reversed-Phase HPLC and Radioactivity Detection of [^{3}H]BYK191023 Incubated with iNOS. Known amounts of [^{3}H]BYK191023 were added to the iNOS preincubation mixture described above. After complete consumption of 1 mM NADPH (detected by disappearance of the 340-nm peak) the enzyme was removed from the mixture by filter centrifugation with a 50-kDa mol. wt. cut-off PVDF membrane. The passed-through solution was collected and analyzed for metabolites by HPLC (Waters model 510 equipped with a Waters 490 multiwavelength detector; Waters, Milford, MA). Chromatograms were obtained on a C18 reversed-phase column (Vydac 218TP54; 5 μm; 4.6 × 250 mm; Grace Vydac, Hesperia, CA) at 280 and 400 nm with (60%) H_2O (0.1% trifluoroacetic acid) and 40% CH_3CN. The flow rate was 1.0 ml/min. The enzyme retained by the filter membrane was washed and filtered again six to eight times with 200 μl of buffer A containing 1.0 mg/ml BSA and high concentrations of Arg (>50 mM). The filtered solution was collected each time and diluted in 2 ml of ECOLITE cocktail (MP Biomedicals, Irvine, CA). Radioactivity was quantified using a PerkinElmer Wallac 1409 liquid scintillation counter (PerkinElmer Life and Analytical Sciences, Waltham, MA). Control experiments were performed by either omitting NADPH or BYK191023 in the preincubation mixture or by introducing BSA instead of iNOS enzyme.

Gel Filtration Chromatography. Samples of 5 μM iNOS (100 μl), incubated for 60 to 120 min as described above, with and without 100 unit/ml SOD, 25 unit/ml catalase, were subjected to gel filtration chromatography on a 30 × 10 cm Superdex 200HR 10/300GL column. The column was equilibrated with 40 mM EPPS buffer, pH 7.6, containing 10% glycerol, 3 mM dithiothreitol, and 150 mM NaCl. Protein in the column effluent was detected at 280 nm using a flow-through UV detector. The molecular weight of the proteins was estimated based on elution profiles of protein standards as described previously (Abu-Soud et al., 1995). Typically, two copies of the gel filtration profiles were made, and the overlapping dimer and monomer peaks were cut out separately from each copy and weighed on a microbalance. The weights of the peaks were used as direct measures of their areas and used to determine the dimer/monomer ratio.

Ferrous Heme-Carbonyl Complex Detection. During iNOS preincubation with BYK191023 and NADPH as described above, the UV-Vis spectra of the dithionite-reduced CO-bound protein was recorded at fixed time. The formation of a peak at 444 nm is distinctive of the CO-heme ferrous complex (P450), and it was used to estimate the heme protein concentration using $\Delta\varepsilon_{444\text{-}500}$ = 74 mM^{-1} cm^{-1} (Adak et al., 1999).

Statistical Analysis. All experiments were repeated three or more times using different batches of proteins purified separately. Data were analyzed and expressed as mean ± S.D. of the mean. Analysis for statistically significant differences among mean values was done, when applicable, using the Student's t test with a value of $p < 0.05$ considered as significant.

Results

Time Course of NOS Inhibition by BYK191023. Binding of BYK191023 to iNOS was demonstrated previously to be L-arginine-competitive and reversible by Strub et al. (2006). Here, we examined the time course of iNOS and nNOS inhibition by BYK191023 over a 60-min period in the absence or in the presence of excess NADPH. Aliquots of a preincubation mixture containing enzyme and substrates as described under *Materials and Methods* were removed at regular intervals, and they were assayed for residual activities using the oxyhemoglobin assay (measuring the instantaneous rate of NO synthesis). Table 1 reports the maximum rate of NO synthesis measured within 10 min after initiating the assay. The data indicate that iNOS undergoes time-dependent inhibition only in the presence of NADPH. In its absence, inhibition was of lower degree and constant during the entire course of preincubation. On the contrary, nNOS showed an equally moderate decrease of NO synthesis (10–20%) both in the presence or absence of NADPH and bound CaM; therefore, nNOS is inefficiently inhibited over time. We also observed that, during the time frame of the assay, iNOS inhibition was irreversible using 100 μM Arg in the mixture; however, it was partially reversible using high Arg concentrations (5 mM), as reported in Table 1. We deduce that BYK191023 acts on iNOS through both a competitive and a time-dependent irreversible mechanism-based inhibition. In the presence of excess NADPH and inhibitor, the time-dependent decrease of iNOS activity well fit to a first-order

exponential decay. The rate constant obtained for the enzyme inactivation is k_{inact} = 0.06 ± 0.01 min^{-1}. Positive control experiments for time-dependent inhibition were performed using the highly selective iNOS inhibitor 1400W (Garvey et al., 1997).

NADPH Consumption/NO Synthesis Ratio during Preincubation. Before preincubation (t = 0 min), the NADPH oxidation supported by iNOS was 211 min^{-1} using arginine alone and 190 min^{-1} in BYK191023-bound iNOS, suggesting that the inhibitor does not affect the electron transfer from NADPH to the flavins in the reductase module. Under normal catalytic conditions, the conversion of Arg to NO requires stoichiometrically 1.5 equivalents of NADPH (Stuehr, 1999). However, before preincubation, the ratio of NADPH oxidized per NO release for iNOS (+,−) was about 2 in absence of bound arginine, in accordance with values reported previously (Alderton et al., 2001). Table 2 shows the NADPH/NO ratio calculated at different time points during preincubation. Once bound to iNOS, BYK191023 competitive inhibition reduced NO synthesis, and, as a result, 4-fold molar excess of inhibitor increased the ratio to 3.3 (t = 1 min). The ratio then gradually increased 10-fold to about 33 at 60 min, suggesting that time-dependent inhibition by BYK191023 separates the NO synthesis from the electron flux derived from NADPH.

Inhibition of iNOS under Anaerobic Conditions. The iNOS steady-state consumption of NADPH quickly depletes oxygen from the air-saturated solution (typically $[O_2]$ <200 μM) if this is not kept in equilibrium with air by mechanical method. We noticed that the onset of the time-dependent iNOS inhibition was significantly delayed if the solution received insufficient air exchange during preincubation. Thus, we hypothesize molecular oxygen to be a component of the irreversible mechanism of inactivation. To test this hypothesis, we preincubated iNOS under anaerobic conditions as described under *Materials and Methods*, and we monitored NO synthesis over time. In Fig. 2, we compared the time course of aerobic (empty circles) and anaerobic inhibition (filled circles). Under anaerobic conditions, the NO synthesis remains nearly constant throughout the whole 60 min of preincubation. The average value obtained (about 63 min^{-1}) was comparable with the NO synthesis inhibition of 10 μM BYK191023 in the absence of NADPH (Table 1). The amount of inhibition can be attributed mostly to the Arg-competitive mechanism. After 60 min of preincubation, we exposed the sample to air, and we observed a considerable reduction of NO synthesis along with simultaneous, slow, oxidation of the NADPH in solution (data not shown). This result supports the hypothesis that oxygen is a critical factor to achieve the time-dependent inactivation of iNOS by BYK191023 and together with the uncoupled NADPH oxidation, let us suppose that formation of superoxide and/or hydrogen peroxide could be responsible for the onset of irreversible iNOS inhibition. Therefore, we repeated the aerobic preincubation experiments adding excess SOD and catalase. Their catalytic function had minimal or no effect on the time-dependent increase of inhibition (Fig. 2, empty triangles). Therefore, a mechanism of inhibition in which reactive oxygen species are released in solution before interaction with iNOS can be excluded. However, we cannot rule out the formation of transitional oxygen reactive species that can react directly with the protein or the heme porphyrin ring.

Spectral Shift upon Binding of Inhibitor. UV-visible spectra of 4 μM inducible oxygenase domain and iNOS full-length (purified in the absence of Arg but containing 10 μM H_4B) were recorded moments before and after the addition of 8 μM BYK191023 in buffer A (see *Materials*) at room temperature. Binding of BYK191023 causes a rapid shift (within minutes) of the heme iron Soret band from a mixed spin-state (peak at 408 nm) to a high-spin state (peak at 396 nm), as evidenced by the spectra reported in Fig. 3 and the difference in the inset. The same spectral shift was obtained adding 100 μM Arg; therefore, BYK191023 bound iNOS was spectrally indistinguishable from Arg-bound iNOS. These spectral changes are consistent with a prompt inhibitor-enzyme interaction, in agreement with the k_{on} value (7200 M^{-1} s^{-1}) reported previously (Strub et al., 2006). For this reason, an inhibition mechanism involving slow binding of BYK191023 to iNOS can be excluded. Furthermore, reduction of the inhibitor bound enzymes with $Na_2S_2O_4$ in the presence of CO produced an absorbance peak at 444 nm (P450) due to the formation of the ferrous heme-thiolate CO complex (such as the spectra recorded at time 0 min in Fig. 9). This result indicates that the inhibitor does not perturb dithionite-mediated heme reduction and the build-up of the ferrous NOS-CO complex.

Determination of Apparent k_{off}. To determine the inhibitor dissociation rate from iNOS, we used a spectroscopic method based on the ability of imidazole, a heme ligand, to bind to iNOS. As shown in Fig. 4, addition of 25 mM imidazole converts the BYK191023-bound iNOS heme iron from a high-spin state (peak at 396 nm) to a low-spin state (peak at

TABLE 1

Time course of NO synthesis during preincubation of 2.5 μM iNOS or nNOS with 10 μM BYK191023

Enzymes were pre-incubated in the absence or presence of NADPH (indicated as − and + NADPH, respectively) as described under *Materials and Methods* and NO synthesis was measured at fixed time at room temperature. To test reversibility of inhibition, iNOS preincubated with NADPH was assayed also in cocktails containing 5 mM Arg (compared with the standard 100 μM Arg). nNOS preincubation included Ca^{2+}/CaM in the mixture. The values represent the mean ± S.D. of at least three separate measurements.

Preincubation Time	NO Synthesis				
	iNOS			nNOS	
	−NADPH	+NADPH 100 mM Arg	+NADPH 5 mM Arg	−NADPH	+ NADPH
		min^{-1}			*min^{-1}*
0 min	97.3 ± 6.2	99.6 ± 5.3	103 ± 7	52.4 ± 3.3	51.8 ± 2.9
15 min	57.2 ± 7.1	25.2 ± 3.7	46 ± 4	47.3 ± 2.8	48.3 ± 1.8
30 min	51.7 ± 5.6	10.2 ± 1.9	32 ± 4	46.1 ± 3.1	43.1 ± 4.1
45 min	50.3 ± 4.8	4.9 ± 5.5	26 ± 2	45.7 ± 2.3	44.3 ± 2.0
60 min	49.2 ± 5.1	2.1 ± 0.4	14 ± 3	44.2 ± 1.8	40.2 ± 2.5

427 nm), and it caused the complete exchange of inhibitor with imidazole in 75 min. We fit the curve of absorbance decrease at 396 nm to a first-order exponential decay to estimate the apparent dissociation rate constant, k_{off}. It was found to be 0.10 ± 0.02 min^{-1}. Nevertheless, we observed that higher concentrations of imidazole caused a quicker decay, indicating that the apparent k_{off} rates that are experimentally attainable were actually slower than the true k_{off}. The association rate k_{on} was previously determined as 7200 M^{-1} s^{-1} (Strub et al., 2006); therefore, using our estimated k_{off}, we obtain K_D = 0.23 μM.

Irreversible Inhibition of iNOS in Intact Cells. To test whether time-dependent irreversible inhibition of iNOS also occurs in intact cells, we incubated iNOS-overexpressing HEK293 and RAW macrophages with BYK191023 after iNOS-induction (as described under *Materials and Methods*), and we determined the residual iNOS activity. After overnight induction of iNOS, HEK293 cells were incubated with various concentrations of BYK191023 for 10 and 30 min, and iNOS activity was measured using the L-[^{3}H]arginine method after careful removal of unbound inhibitor before cell lysis. Figure 5A shows a concentration-dependent irreversible inhibition of iNOS activity from 29 to 86% after 10 min of preincubation with BYK191023. After 30 min of preincubation with BYK191023, a nearly complete irreversible inhibition of iNOS activity was found at any concentration used (Fig. 5A). The efficacy of inhibitor removal before cell lysis was determined in a separate experiment. After two wash steps, 99.2 to 99.4% of radioactivity and after three wash steps, 99.4 to 99.9% of radiolabeled BYK191023 was removed, suggesting that the final cellular concentrations of

TABLE 2
NADPH oxidation, NO synthesis, and their ratio during preincubation of iNOS

Steady-state activities were measured during the time-dependent onset of inhibition with the oxyhemoglobin assay as described under *Materials and Methods*. Time point 0 indicates rates before initiating preincubation with 10 μM BYK191023 and 1 mM NADPH.

Preincubation Time	NADPH Oxidation	NO Synthesis	NADPH/NO Ratio
	min^{-1}		
0 min	211 ± 9.8	99.6 ± 5.3	2.1
1 min	190 ± 7.6	56.4 ± 5.8	3.3
10 min	155 ± 7.1	27.7 ± 2.4	5.6
20 min	98 ± 5.5	11.3 ± 2.1	9.0
30 min	72 ± 6.0	5.2 ± 1.6	13.8
60 min	57 ± 4.3	1.7 ± 1.1	33.5

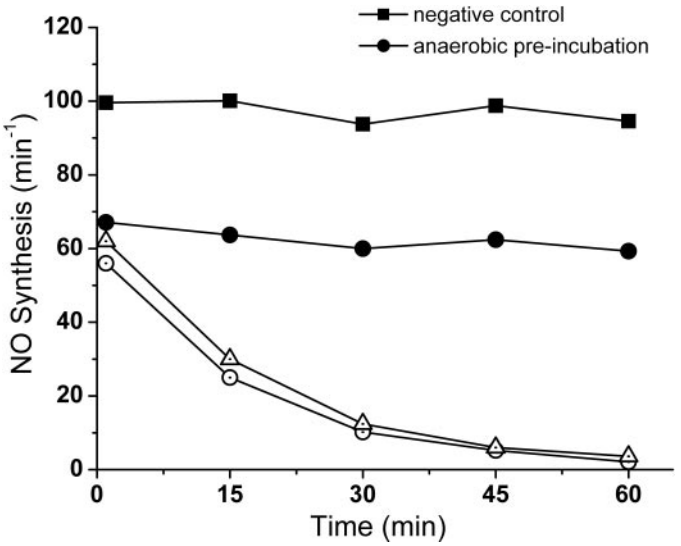

Fig. 2. Time and oxygen dependence of iNOS inhibition by BYK191023. Murine iNOS (2.5 μM) was preincubated for the indicated time with 10 μM BYK191023 and 1 mM NADPH at room temperature as described under *Materials and Methods*. Rates of NO synthesis were determined using the oxyhemoglobin assay. Empty circles (○) and triangles (△) indicate, respectively, that superoxide dismutase and catalase were absent or present in the preincubation mixture. Filled circles (●) represent activity measurements during anaerobic preincubation of iNOS. The data are the mean of three independent experiments. Negative control (■) indicates that iNOS was preincubated in the absence of inhibitor.

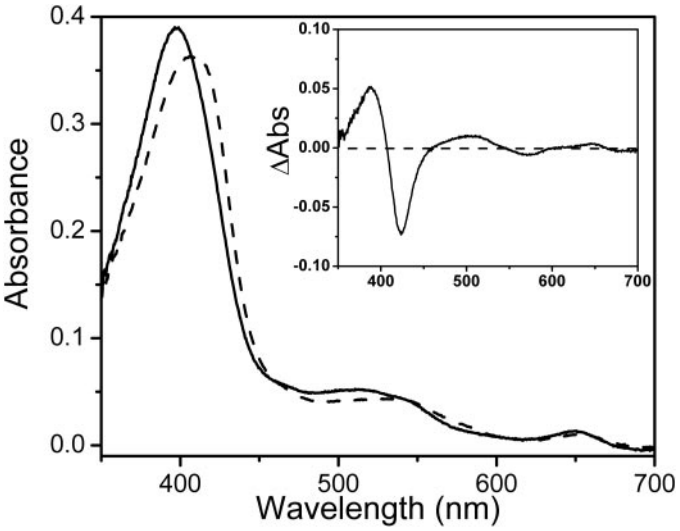

Fig. 3. Visible absorbance spectra of iNOS (−Arg, +H_4B) before and after the binding of BYK191023. The Soret shift from 408 to 396 nm indicates that preincubation with BYK191023 induces a spin state transition of the heme iron equivalent to that obtained with arginine. The inset shows the difference spectra generated by subtracting the initial spectrum (- - -) from that recorded after binding of BYK191023 (—).

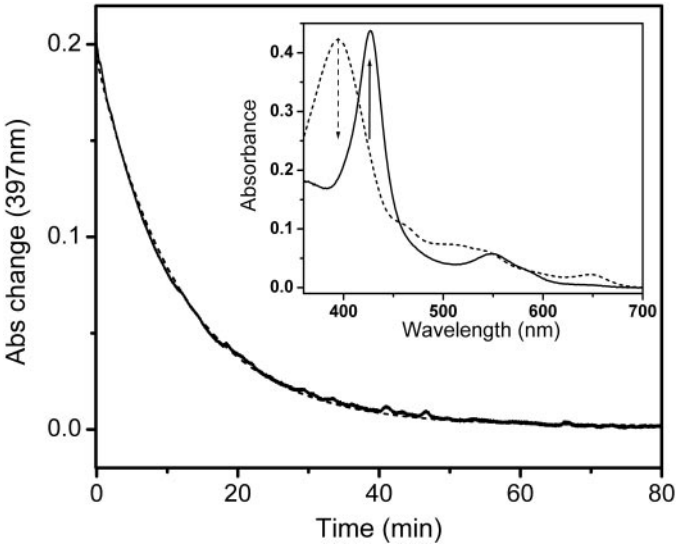

Fig. 4. Kinetics of BYK191023 dissociation. BYK191023 dissociation measured after the addition of 25 mM imidazole was followed spectrally by monitoring the absorbance decrease at 397 nm. The imidazole displaced BYK191023 completely in about 70 min. The curve was fitted using a first-order exponential decay equation to determine the apparent k_{off}. The inset shows the initial spectrum of BYK191023 bound iNOS (- - -) and 80 min after addition of 25 mM imidazole (—). Imidazole binding to iNOS converts the heme iron from a high-spin state (Soret peak at 396 nm) to a low-spin state (Soret peak at 427 nm).

BYK191023 are far lower than its cellular IC_{50} value (13.6 μM) at HEK293 iNOS cells (Strub et al., 2006), even at highest concentrations used. Similar results were found using murine RAW macrophages. RAW macrophages were incubated with 100 μM BYK191023 after iNOS stimulation (as described under *Materials and Methods*). NO synthesis was directly determined using a NO-selective microelectrode. In Fig. 5B, we compared the percentage of NO released by the cells after washing out the inhibitor or in the presence of inhibitor. After 10 min of preincubation with BYK191023, the iNOS activity was reduced by about 75% relative to the control; however, after 30 min complete irreversible inhibition of iNOS activity was measured (Fig. 5B). Samples containing 100 μM BYK191023 in the activity assay were included as positive controls, indicating that we indeed determined the release of iNOS-mediated nitric oxide (Fig. 5B). Thus, also in intact cells, BYK191023 irreversibly inhibits iNOS in a time-dependent manner.

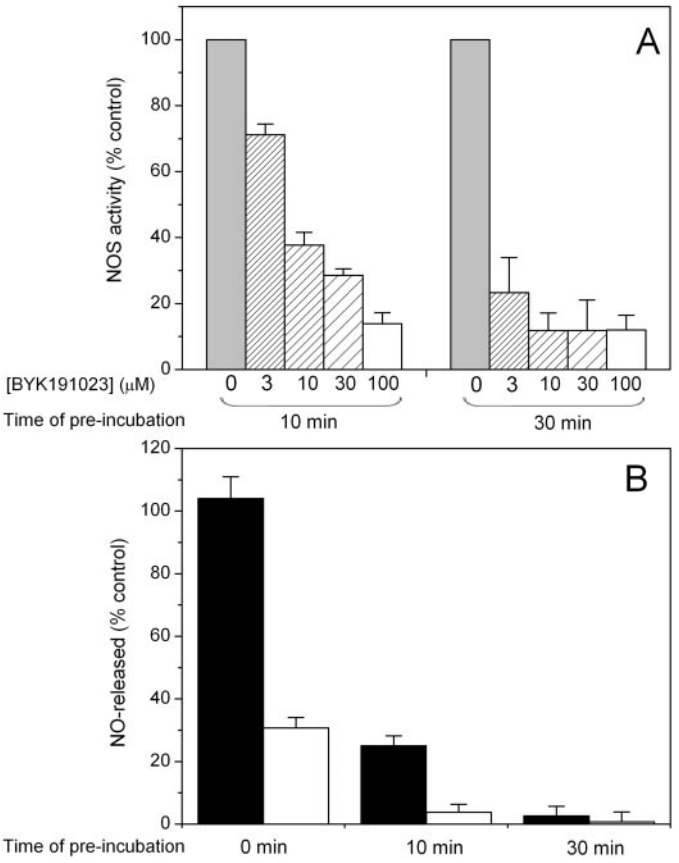

Fig. 5. Time-dependent irreversible inhibition of cellular iNOS by BYK191023 in HEK293 iNOS and RAW macrophages. A, after ponasterone A-mediated overnight induction of iNOS, HEK293 iNOS cells were incubated with the indicated concentrations of BYK191023 for 10 and 30 min. Before cell lysis, the unbound inhibitor was removed by washing the intact cells three times with medium. iNOS activity was measured using the L-[^{3}H]arginine method, and activity is shown as percentage of control activity (means ± S.E.M.; n = 3). B, RAW macrophages were incubated as cellular suspension at 37°C with 100 μM BYK191023 for the indicated time after overnight induction of iNOS by LPS and IFN-γ. After preincubation, cells were washed, resuspended in buffer without inhibitor (black bars) or 100 μM BYK191023 (white bars), and NO release was quantified using a NO-sensitive microelectrode. A negative control incubated without inhibitor was used to determine the maximal NO synthesis rate as control. The rates of NO release reported are in percentage of control activity (means ± S.E.M.; n = 4–6).

[^{3}H]BYK191023 Dissociation from Inactivated iNOS. iNOS was preincubated with [^{3}H]BYK191023 as in aerobic experiments for 60 min, and then it was washed with buffer A (200 μl) containing indicated Arg and 1.0 mg/ml bovine BSA to increase the enzyme stability. The enzyme was separated from the mixture using a 50-kDa mol. wt. cut-off PVDF membrane, and the radioactivity in the flow-through was measured by liquid scintillation counting. The process was repeated until only background scintillation could be detected in the filtered solution. Figure 6 represents the total amount of counts (dpm) versus the volume of buffer used to wash iNOS proteins. More than 97% of [^{3}H]BYK191023 was recovered in the filtrate after seven washes with buffer alone (1.4 ml); however, when high concentrations of Arg (>100 mM) were used, the dissociation of BYK191023 from iNOS was more efficient. BSA was used as a substitute for iNOS to monitor unspecific BYK191023 protein binding (negative control). Approximately 90% of the radioactive inhibitor used was recovered after the first wash and 95% after the second wash. We conclude that BYK191023 formed no significant covalent bond with the protein during preincubation with NADPH; however, the results confirm that its dissociation is a slow process, as shown previously (Fig. 4). We also measured NO synthesis in samples after extensive washes with Arg (data not shown). We observed only partial recovery of activity compared with preincubation mixtures used as controls and containing either no NADPH or no BYK191023. This result confirms the irreversible inactivation of iNOS after NADPH consumption.

Gel Filtration Chromatography of Inactivated iNOS. Dimerization of purified heme-containing iNOS monomers is essential for activity, and it is promoted by the presence of H_4B and Arg. A series of potent and selective NOS inhibitors have been shown to prevent enzyme dimerization in cells and to inhibit iNOS in vitro and in vivo (Blasko et al., 2002). BYK191023 does not show any structural similarity to these

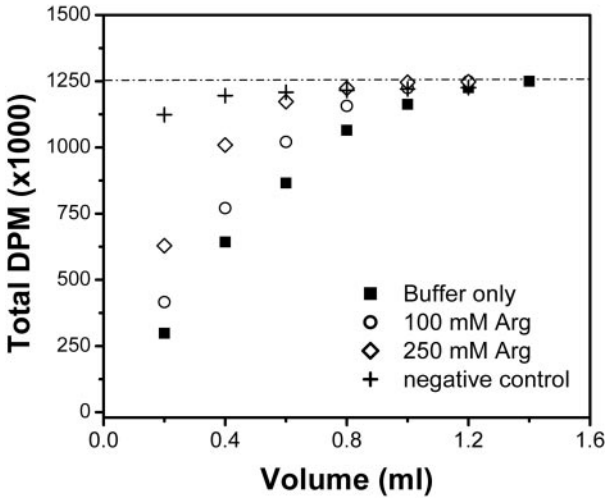

Fig. 6. Dissociation of [^{3}H]BYK191023 from inactivated iNOS. iNOS (2.5 μM) was incubated with 0.2 μCi of [^{3}H]BYK191023, 1 mM NADPH, and 0 to 10 μM unlabeled BYK191023 for 1 h at 25°C. Each reaction mixture was filtered through a PVDF membrane to remove unbound radioligand and counted. The enzyme retained by the membrane was washed and filtered again five to eight times with 200 μl of buffer A containing 1.0 mg/ml BSA and different concentrations of Arg. The solutions were collected each time, and radioactivity was quantitated by a scintillation counter (as described under *Materials and Methods*). Data are means of three replicates.

compounds. However, we analyzed BYK191023 acting at dimeric iNOS and irreversibly inhibiting iNOS by promoting dissociation into monomers; therefore, we investigated its dimeric structure by gel filtration chromatography. Trace 1 in Fig. 7 shows that iNOS after preincubation in the absence of NADPH is almost entirely in dimeric form (about 98%), as judged from comparison with Arg and H_4B-bound iNOS (data not shown). Trace 2 (Fig. 7) represents the elution profile of iNOS after 60-min preincubation with 1 mM NADPH, and it reveals a partial transformation to the inactive monomer (21% of the total amount of iNOS loaded). At the end of preincubation, we added 5 mM Arg to the mixture, and the monomer/dimer ratio was monitored again after 3, 6, and 12 h: the percentage of monomer increased to reach a maximum of about 45% of the total iNOS at 6 h, and then other degeneration processes, independent of the inhibitor presence, seemed to take place (data not shown).

BYK191023 Irreversible Inhibition of iNOS Causes Loss of Heme. Inhibitor-treated, inactivated iNOS was washed with buffer A containing 5 mM Arg, for 80 min to dissociate bound BYK191023. Then, the enzyme was separated by filter centrifugation with a 50-kDa mol. wt. cut-off membrane before injecting the filtrate solution into a reverse-phase HPLC column. To identify the dissociated products, UV-visible absorption chromatograms were recorded at 280 and 400 nm, as shown in Fig. 8, A and B, respectively. The fraction with elution time around 2 to 3 min corresponds to a mixture of NADPH, $NADP^+$, and H_4B that are present in high concentration and detected in both chromatograms. In Fig. 8A, the peak eluting at 12 min corresponds to native BYK191023, whereas in Fig. 8B, the major peak (20–23 min) eluted comparably to pure commercial hemin. Control solutions prepared omitting either inhibitor or NADPH did not lead to heme loss. In the samples, we detected other very low-level 400-nm-absorbing compounds visible only using higher gain in the detector. We attempted to identify possible NADPH- and time-dependent formation of biliverdin, as suggested by the 1400W inactivation of iNOS (Zhu et al., 2005), but differences with the retention time of commercial biliverdin precluded an accurate identification. We then collected HPLC fractions from [^{3}H]BYK191023 inactivated iNOS every 0.5 min, and we detected radioactivity for each fraction by scintillation. Radioactivity was associated exclusively with the elution time of unmodified inhibitor. Therefore, we ruled out the generation of inhibitor metabolites or a covalent interaction with the enzyme.

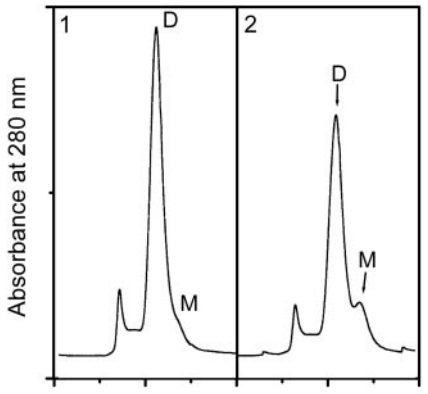

Fig. 7. Gel filtration profiles demonstrating the effect on the dimer/monomer ratio of BYK191023-bound iNOS during onset of irreversible inhibition. One hundred microliters of solution containing 3 μM iNOS was loaded on Superdex 200HR column as described under *Materials and Methods*. Trace 1, the protein after preincubation with BYK191023 but in the absence of NADPH. The single iNOS peak is entirely in dimeric form. Trace 2, the elution profile after preincubation with 5 mM Arg after 60-min preincubation with BYK191023 and NADPH. D and M indicate, respectively, dimeric or monomeric iNOS. The results shown are representative of three independent experiments.

Characterization of the Ferrous Heme-CO Complex. We acquired spectra of iNOS at fixed times during the preincubation immediately after addition of dithionite and slowly bubbling CO in the cuvette (Fig. 9). Initially, the dithionite-reduced NOS heme iron directly binds CO to form only the distinctive ferrous heme-CO complex (P450) (White and Marletta, 1992). However, after 15 min the spectra obtained already revealed simultaneous formation of P420 species, a dysfunctional form of the enzyme-bound heme. The inset of Fig. 9 illustrates the time dependence of the P450 and P420 formation. During the first 15 min, the decrease of the P450 peak correlates with the increase in the P420 peak, and the total amount of heme in the enzyme remained constant. This implies a chemical change of the heme as a consequence of ligand shift or protonation of the thiolate proximal ligand. Afterward, the decreasing ability of iNOS to form any heme-CO complex correlates well with the irreversible loss of NOS activity and the detection by HPLC of free heme. In Table 3, we estimated the heme protein concentration at each time point from the P450 ($\Delta\varepsilon_{444\text{-}500}$ = 74 mM^{-1} cm^{-1}).

Discussion

The imidazopyridine derivate BYK191023 was previously identified as a selective and Arg-competitive inhibitor of

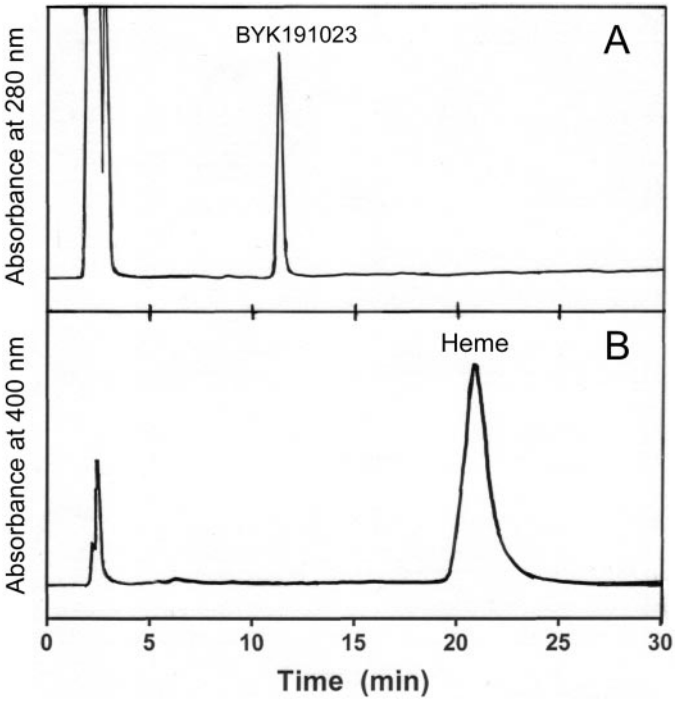

Fig. 8. HPLC analysis of inactivated iNOS after dissociation of BYK191023 and filtration. A, chromatogram recorded at 280 nm shows the peak at 12 min corresponding to the elution time for native BYK191023. B, chromatogram recorded at 400 nm showing the major fraction eluting at 20 to 23 min and equivalent to pure commercial hemin. The fraction with elution time around 2 to 3 min corresponds to a mixture of NADPH, $NADP^+$, and H_4B, and it is detected in both chromatograms.

iNOS (Strub et al., 2006). The present study shows that when operating in the absence of Arg (or after depletion), BYK191023 is an NADPH and oxygen time-dependent irreversible iNOS inhibitor that leads to loss of the heme prosthetic group.

Characterization of BYK191023 Interaction with iNOS. Arginine binds above the plane of NOS heme isozymes (Wang et al., 1993), and it shifts its heme iron toward a high-spin configuration, as shown by Soret band changes in the visible spectrum (McMillan and Masters, 1993). The spectra of iNOS incubated with BYK191023 (Fig. 4) were indistinguishable from that of Arg-bound iNOS, indicating that the inhibitor-enzyme interaction (probably in proximity to the Arg binding site) alters the heme iron spin equilibrium in the same way. The active site of all NOS, known in detail from a number of X-ray crystal structures (Crane et al., 1998; Ortiz de Montellano et al., 1998), is an iron-protoporphyrin IX center coordinated to a cysteine thiolate that binds and activates molecular oxygen (O_2). Binding of cofactors H_4B and Arg to iNOS is accompanied by the conversion of the ferric heme iron from a hexacoordinate low-spin (peak centered near 420 nm) to a pentacoordinate high-spin state (peak at 395 nm). Adding excess imidazole reverses the effect and results in a spectral shift to the low-spin state (peak at 427 nm). We used this spectral perturbation method in BYK191023-bound iNOS to calculate the apparent k_{off} (0.10 ± 0.02 min^{-1}) (Fig. 4). The data indicate that the binding of BYK191023 is reversible under these conditions and the slow off-rate of BYK191023 is the principal determinant of competitive inhibition in the absence of preincubation with NADPH.

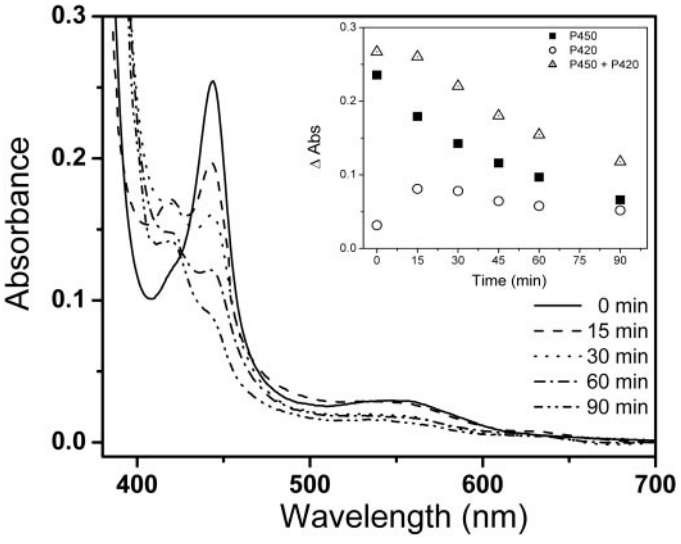

Fig. 9. Formation of the CO-heme ferrous complex (P450) and its conversion to P420 species during iNOS inactivation. Absorbance spectra of 3 μM iNOS were recorded during inactivation of iNOS with BYK191023. The spectra show the change of the peak over time at 444 and 420 nm. The inset represents the variation of the P450 and P420 species and their sum during the time of preincubation with NADPH and inhibitor. All experiments were performed in CO-saturated 40 mM EPPS, pH 7.6. Data shown are representative of three individual experiments.

TABLE 3

Heme ferrous-CO complex concentration during iNOS inactivation by BYK191023

The amount of ferrous heme-CO complex at each time point was calculated from the absorbance peak at 444 nm using $\Delta\epsilon_{444\text{-}500}$ = 74 mM^{-1} cm^{-1}. The concentration decrease correlates with the loss of heme during iNOS inactivation. The data is representative of three independent experiments.

Preincubation Time	P450 Complex
	μM
0 min	3.0
15 min	2.3
30 min	1.8
45 min	1.4
60 min	1.1
90 min	0.8

Preincubation with NADPH Leads to Irreversible iNOS Inhibition. When iNOS is incubated with BYK191023 and high concentrations of NADPH (>100-fold the enzyme), irreversible inhibition develops over time (Table 1; Fig. 2). The inactivation constant calculated by fitting the data to a first-order exponential decay is k_{inact} = 0.06 ± 0.01 min^{-1}. Air exchange by mechanical methods is also necessary to achieve enzyme inactivation. Subsequent anaerobic experiments established that oxygen is a limiting reagent of the onset of irreversible inhibition, and they suggested that it is involved in the mechanism of inactivation.

Irreversible Inhibition in Intact Cells. The time-dependent, irreversible inhibitory effect observed for BYK191023 in vitro was proven to be relevant in two cellular iNOS models. In HEK293 cells overproducing human iNOS, a time- and concentration-dependent inhibition of iNOS activity was found under conditions of nearly complete removal of BYK191023 before cell lysis (Fig. 5A). Likewise, after stimulation of RAW264.7 macrophages by LPS and IFN-γ, iNOS-mediated NO synthesis decreased when the cells were preincubated for increasing times with BYK191023 (Fig. 5B). Thus, the irreversible inhibition by BYK191023 also translates to in vivo cellular cultures.

Possible Mechanisms of Irreversible Inhibition. At least three different mechanisms could explain the irreversible inactivation of iNOS: 1) a time-dependent suicide mechanism is involved wherein the inhibitor is metabolized to a reactive intermediate that covalently binds the enzyme; 2) bound inhibitor may decrease stability of the iNOS dimer by steric effect and induce a time-dependent loss of dimerization [the dimer stability order is iNOS < nNOS ≪ eNOS (Panda et al., 2002) also in accordance with BYK191023 selectivity]; and 3) uncoupled NADPH oxidation in the inhibitor bound iNOS results in the formation of reactive oxygen species at the heme site, and these may cause alteration and/or loss of the porphyrin ring, as reported previously for 1400W and other NOS inhibitors (Demady et al., 2001; Lee et al., 2005; Zhu et al., 2005).

Our data suggest that the first and second mechanism proposed could be excluded or, in any case, are not the main processes responsible for enzyme inactivation. The first mechanism implies the generation of inhibitor metabolites and/or a direct enzyme-inhibitor covalent interaction, but it is in contrast with two main results. We recovered [^{3}H]BYK191023 quantitatively after full iNOS inactivation (Fig. 6), and the radioactivity of HPLC fractions was associated exclusively with the elution time of the unmodified inhibitor. The second mechanism can account for the enzyme inactivation only partially: size exclusion chromatography traces revealed about 20% iNOS dissociation into monomers after 60 min of preincubation (Fig. 7). Hence, the limited iNOS monomerization during preincubation cannot account for the irreversible inhibition. Moreover, in Fig. 9 we show that the enzyme inactivation is associated with the appear-

ance of an iNOS P420 species that represents a five-coordinate ferrous-CO complex in which the cysteine ligand has been weakened or dissociated from the heme iron. The heme-thiolate bond is essential for NOS to dimerize (Hemmens et al., 1998); therefore, the monomerization process should be considered rather a consequence than the cause of inactivation. In addition, the cofactor H_4B is known to be critical for stabilizing iNOS dimeric structure (Baek et al., 1993); however, our experiments were performed in the presence of 10 μM H_4B, and its limited availability can be excluded.

Only the third proposed mechanism can account for the loss of the enzyme heme detected by HPLC (Fig. 8B) and for the time-dependent P450-P420 complex conversion, and it includes the requirement of oxygen. As in other cytochromes P450, the formation of a P420 species is diagnostic of the generation of an inactive enzyme, and the process is often irreversible (Huang et al., 1999; Nebbia et al., 1999). Therefore, the presence of BYK191023 together with the "uncoupled" electron flux from NADPH seems to destabilize the iron-cysteine bond. During the normal NOS catalytic cycle, the electrons provided by NADPH are transferred to the heme iron, which allows it to bind and activate molecular oxygen. One of the bound oxygen atoms is incorporated into the terminal guanidine nitrogen of Arg with concurrent transformation of the other oxygen atom to H_2O. This reaction is said to be "coupled" when all the electrons are used in the formation of the mono-oxygenated product and H_2O. At concentrations of Arg below NOS k_m ($\approx$5 μM), electrons are still transferred to the heme iron, but bound oxygen cannot efficiently react with the substrate. Instead, superoxide radicals and other reactive oxygen species (ROS) such as hydrogen peroxide are produced. This phenomenon is called uncoupling, and abundant evidence is provided by electron paramagnetic resonance spin trap (Gao et al., 2007). Addition of excess amounts of SOD and catalase scavenge superoxide and H_2O_2 released in solution (Misra and Fridovich, 1972). Uncoupled NOS catalytic activity can occur naturally due to a decline in the cofactor H_4B (Wei et al., 2003), but it has also been observed in the presence of N^G-monomethyl-L-arginine, an endogenous inhibitor of NOS (Olken and Marletta, 1993). Under pathophysiological conditions, Arg levels are strongly decreased in human serum (Morris et al., 2004; Zimmermann and Rothenberg, 2006) and decreased up to 1000-fold in rat serum after LPS treatment (A. Strub and M. D. Lehner, unpublished observations), thus limiting substrate availability for iNOS. NADPH levels are only slightly elevated under pathophysiological conditions (Morris et al., 2008). During the preincubation of the enzyme with BYK191023, the ratio of NADPH oxidized per NO release increased 10-fold. This suggests that the inhibitor presence in the vicinity of the heme enhances production of reactive oxygen species. However, addition of SOD and catalase to the preincubation mixture had no significant effect on diminishing iNOS inactivation (Fig. 2) or heme loss (Fig. 8). The process then seems not to be related to the accumulation of ROS in solution. Studies on the inhibitor 1400W reported that the mechanism of iNOS inactivation by this compound is related to the mechanism of the enzyme heme oxygenase (Zhu et al., 2005). The iron-peroxide intermediate formed reacts with the porphyrin ring, resulting its conversion to biliverdin. We looked for this metabolite in our system by HPLC after iNOS inactivation with BYK191023, but it was undetectable. Thus, the specific role of any ROS species generated by inhibitor bound iNOS during its inactivation is not clear; however, the crystal structure of BYK191023 bound iNOS will help to elucidate this question, because heme surrounding protein structure would determine the possible kinetics of the reactions.

In conclusion, our study establishes that BYK191023 inhibits iNOS through two different pathways: one pathway, in the absence of or limited NADPH, is a competitive mechanism involving decreased NO synthesis via antagonism of Arg binding. The other pathway operates after Arg depletion, or below micromolar Arg levels, and it is an NADPH- and time-dependent irreversible inhibition associated with perturbations of the heme iron environment. In vivo, Arg levels are variable and often limit NOS activity in cells and tissues, also due to arginase expression (Zhang et al., 2004), so it should be considered that both mechanisms can operate at the same time. Enzyme inactivation is correlated with the loss of the incorporated heme moiety that accounts for at least two thirds of the NOS activity lost. No metabolites were detected using radiolabel inhibitor; thus, BYK191023 is a new example of a compound that causes irreversible inactivation of an enzyme without becoming itself modified.

Acknowledgments

We thank Deborah Durra, Elisabeth Herrmann, Tina Geppert, and Jeannette Keller for expert technical assistance; Dr. Koustubh Panda for stimulating discussions; and Dr. Mohammad Mahfuzul Haque for manuscript revision.

References

Abu-Soud HM, Loftus M, and Stuehr DJ (1995) Subunit dissociation and unfolding of macrophage NO synthase: relationship between enzyme structure, prosthetic group binding, and catalytic function. *Biochemistry* **34:**11167–11175.

Adak S, Ghosh S, Abu-Soud HM, and Stuehr DJ (1999) Role of reductase domain cluster 1 acidic residues in neuronal nitric-oxide synthase. Characterization of the FMN-FREE enzyme. *J Biol Chem* **274:**22313–22320.

Alderton WK, Cooper CE, and Knowles RG (2001) Nitric oxide synthases: structure, function and inhibition. *Biochem J* **357:**593–615.

Baek KJ, Thiel BA, Lucas S, and Stuehr DJ (1993) Macrophage nitric oxide synthase subunits. Purification, characterization, and role of prosthetic groups and substrate in regulating their association into a dimeric enzyme. *J Biol Chem* **268:** 21120–21129.

Blasko E, Glaser CB, Devlin JJ, Xia W, Feldman RI, Polokoff MA, Phillips GB, Whitlow M, Auld DS, McMillan K, et al. (2002) Mechanistic studies with potent and selective inducible nitric-oxide synthase dimerization inhibitors. *J Biol Chem* **277:**295–302.

Crane BR, Arvai AS, Ghosh DK, Wu C, Getzoff ED, Stuehr DJ, and Tainer JA (1998) Structure of nitric oxide synthase oxygenase dimer with pterin and substrate. *Science* **279:**2121–2126.

Demady DR, Jianmongkol S, Vuletich JL, Bender AT, and Osawa Y (2001) Agmatine enhances the NADPH oxidase activity of neuronal NO synthase and leads to oxidative inactivation of the enzyme. *Mol Pharmacol* **59:**24–29.

Gao YT, Panda SP, Roman LJ, Martasek P, Ishimura Y, and Masters BS (2007) Oxygen metabolism by neuronal nitric-oxide synthase. *J Biol Chem* **282:**7921–7929.

Garvey EP, Oplinger JA, Furfine ES, Kiff RJ, Laszlo F, Whittle BJ, and Knowles RG (1997) 1400W is a slow, tight binding, and highly selective inhibitor of inducible nitric-oxide synthase in vitro and in vivo. *J Biol Chem* **272:**4959–4963.

Hemmens B, Gorren AC, Schmidt K, Werner ER and Mayer B (1998) Haem insertion, dimerization and reactivation of haem-free rat neuronal nitric oxide synthase. *Biochem J* **332:**337–342.

Hobbs AJ, Higgs A, and Moncada S (1999) Inhibition of nitric oxide synthase as a potential therapeutic target. *Annu Rev Pharmacol Toxicol* **39:**191–220.

Huang L, Abu-Soud HM, Hille R, and Stuehr DJ (1999) Nitric oxide-generated P420 nitric oxide synthase: characterization and roles for tetrahydrobiopterin and substrate in protecting against or reversing the P420 conversion. *Biochemistry* **38:** 1912–1920.

Lechner M, Lirk P, and Rieder J (2005) Inducible nitric oxide synthase (iNOS) in tumor biology: the two sides of the same coin. *Semin Cancer Biol* **15:**277–289.

Lee AJ, Noon KR, Jianmongkol S, Lau M, Jenkins GJ, and Osawa Y (2005) Metabolism of aminoguanidine, diaminoguanidine, and NG-amino-L-arginine by neuronal NO-synthase and covalent alteration of the heme prosthetic group. *Chem Res Toxicol* **18:**1927–1933.

Lehner MD, Marx D, Boer R, Strub A, Hesslinger C, Eltze M, Ulrich WR, Schwoebel F, Schermuly RT, and Barsig J (2006) In vivo characterization of the novel imidazopyridine BYK191023 [2-[2-(4-methoxy-pyridin-2-yl)-ethyl]-3*H*-imi-

dazo[4,5-*b*]pyridine], a potent and highly selective inhibitor of inducible nitric-oxide synthase. *J Pharmacol Exp Ther* **317:**181–187.
Li H and Forstermann U (2000) Nitric oxide in the pathogenesis of vascular disease. *J Pathol* **190:**244–254.
McMillan K and Masters BS (1993) Optical difference spectrophotometry as a probe of rat brain nitric oxide synthase heme-substrate interaction. *Biochemistry* **32:** 9875–9880.
Michel T and Feron O (1997) Nitric oxide synthases: which, where, how, and why? *J Clin Invest* **100:**2146–2152.
Misra HP and Fridovich I (1972) The generation of superoxide radical during the autoxidation of hemoglobin. *J Biol Chem* **247:**6960–6962.
Moore DJ, West AB, Dawson VL, and Dawson TM (2005) Molecular pathophysiology of Parkinson's disease. *Annu Rev Neurosci* **28:**57–87.
Morris CR, Poljakovic M, Lavrisha L, Machado L, Kuypers FA, and Morris SM Jr (2004) Decreased arginine bioavailability and increased serum arginase activity in asthma. *Am J Respir Crit Care Med* **170:**148–153.
Morris CR, Suh JH, Hagar W, Larkin S, Bland DA, Steinberg MH, Vichinsky EP, Shigenaga M, Ames B, Kuypers FA, et al. (2008) Erythrocyte glutamine depletion, altered redox environment, and pulmonary hypertension in sickle cell disease. *Blood* **111:**402–410.
Nebbia C, Ceppa L, Dacasto M, and Carletti M (1999) Triphenyltin acetate-mediated in vitro inactivation of rat liver cytochrome P-450. *J Toxicol Environ Health A* **56:**433–447.
Olken NM and Marletta MA (1993) NG-methyl-L-arginine functions as an alternate substrate and mechanism-based inhibitor of nitric oxide synthase. *Biochemistry* **32:**9677–9685.
Ortiz de Montellano PR, Nishida C, Rodriguez-Crespo I, and Gerber N (1998) Nitric oxide synthase structure and electron transfer. *Drug Metab Dispos* **26:**1185–1189.
Paige JS and Jaffrey SR (2007) Pharmacologic manipulation of nitric oxide signaling: targeting NOS dimerization and protein-protein interactions. *Curr Top Med Chem* **7:**97–114.
Panda K, Rosenfeld RJ, Ghosh S, Meade AL, Getzoff ED, and Stuehr DJ (2002) Distinct dimer interaction and regulation in nitric-oxide synthase types I, II, and III. *J Biol Chem* **277:**31020–31030.
Strub A, Ulrich WR, Hesslinger C, Eltze M, Fuchss T, Strassner J, Strand S, Lehner MD, and Boer R (2006) The novel imidazopyridine 2-[2-(4-methoxy-pyridin-2-yl)-ethyl]-3H-imidazo[4,5-b]pyridine (BYK191023) is a highly selective inhibitor of the inducible nitric-oxide synthase. *Mol Pharmacol* **69:**328–337.
Stuehr DJ (1996) Purification and properties of nitric oxide synthases. *Methods Enzymol* **268:**324–333.
Stuehr DJ (1999) Mammalian nitric oxide synthases. *Biochim Biophys Acta* **1411:** 217–230.
Tiso M, Konas DW, Panda K, Garcin ED, Sharma M, Getzoff ED, and Stuehr DJ (2005) C-terminal tail residue Arg1400 enables NADPH to regulate electron transfer in neuronal nitric-oxide synthase. *J Biol Chem* **280:**39208–39219.
Wang J, Stuehr DJ, Ikeda-Saito M, and Rousseau DL (1993) Heme coordination and structure of the catalytic site in nitric oxide synthase. *J Biol Chem* **268:**22255–22258.
Wei CC, Crane BR, and Stuehr DJ (2003) Tetrahydrobiopterin radical enzymology. *Chem Rev* **103:**2365–2383.
White KA and Marletta MA (1992) Nitric oxide synthase is a cytochrome P-450 type hemoprotein. *Biochemistry* **31:**6627–6631.
Xu W, Liu LZ, Loizidou M, Ahmed M, and Charles IG (2002) The role of nitric oxide in cancer. *Cell Res* **12:**311–320.
Zhang C, Hein TW, Wang W, Miller MW, Fossum TW, McDonald MM, Humphrey JD, and Kuo L (2004) Upregulation of vascular arginase in hypertension decreases nitric oxide-mediated dilation of coronary arterioles. *Hypertension* **44:**935–943.
Zhu Y, Nikolic D, Van Breemen RB, and Silverman RB (2005) Mechanism of inactivation of inducible nitric oxide synthase by amidines. Irreversible enzyme inactivation without inactivator modification. *J Am Chem Soc* **127:**858–868.
Zimmermann N and Rothenberg ME (2006) The arginine-arginase balance in asthma and lung inflammation. *Eur J Pharmacol* **533:**253–262.

Address correspondence to: Dr. Dennis J. Stuehr, Department of Pathobiology, NC-20, The Cleveland Clinic, 9500 Euclid Ave., Cleveland, OH 44195. E-mail: stuehrd@ccf.org or Dr. Andreas Strub, Nycomed, Byk-Gulden-Str. 2, 78467, Konstanz, Germany. E-mail: andreas.strub@nycomed.com